ADVANCED
FUNCTIONAL
MATERIALS
www.afm-journal.de

Materials
Views
www.MaterialsViews.com

FULL PAPER

Influence of Molecular Geometry of Perylene Diimide Dimers and Polymers on Bulk Heterojunction Morphology Toward High-Performance Nonfullerene Polymer Solar Cells

Chen-Hao Wu, Chu-Chen Chueh, Yu-Yin Xi, Hong-Liang Zhong, Guang-Peng Gao, Zhao-Hui Wang, Lilo D. Pozzo, Ten-Chin Wen, and Alex K.-Y. Jen*

In this study, we investigate the influence of molecular geometry of the donor polymers and the perylene diimide dimers (di-PDIs) on the bulk heterojunction (BHJ) morphology in the nonfullerene polymer solar cells (PSCs). The results reveal that the pseudo 2D conjugated poly[4,8-bis(5-(2-ethylhexyl)thiophen-2-yl)benzo[1,2-b;4,5-b']dithiophene-2,6-diyl-alt-(4-(2-ethylhexyl)-3-fluorothieno[3,4-b]thiophene-)-2-carboxylate-2-6-diyl)] (PTB7-Th) has better miscibility with both bay-linked di-PDI (B-di-PDI) and hydrazine-linked di-PDI (H-di-PDI) compared to its 1D analog, poly[[4,8-bis[(2-ethylhexyl)oxy]benzo[1,2-b:4,5-b']dithiophene-2,6-diyl][3-fluoro-2-[(2-ethylhexyl)carbonyl]thieno[3,4-b]thiophenediyl]] (PTB7), to facilitate more efficient exciton dissociation in the BHJ films. However, the face-on oriented π–π stacking of PTB7-Th is severely disrupted by the B-di-PDI due to its more flexible structure. On the contrary, the face-on oriented π–π stacking is only slightly disrupted by the H-di-PDI, which has a more rigid structure to provide suitable percolation pathways for charge transport. As a result, a very high power conversion efficiency (PCE) of 6.41% is achieved in the PTB7-Th:H-di-PDI derived device. This study shows that it is critical to pair suitable polymer donor and di-PDI-based acceptor to obtain proper BHJ morphology for achieving high PCE in the nonfullerene PSCs.

1. Introduction

To date, the state-of-the-art fullerene-based polymer solar cells (PSCs) have been proved to achieve the power conversion efficiencies (PCEs) exceeding 10%.[1] However, despite this high efficiency, fullerene derivatives suffer from limited spectral breadth, inferior ambient stability, and higher production cost. In this regard, nonfullerene acceptors have been vigorously explored in recent years to replace the commonly used fullerene derivatives for high-performance PSCs.[2] To date, numerous small-molecule nonfullerene acceptors have been reported based on different π-conjugated moieties, such as vinazene, fluoranthene-fused imide, diketopyrrolopyrrole, naphthalene diimide, and perylene diimide (PDI).[3] Among these, the PDI derivatives are the most extensively investigated n-type materials for nonfullerene PSCs due to their intense light absorption, high-electron mobility, decent thermal stability, and relative ease of functionalization.[2,3e] However, the strong tendency for them to form microscale aggregates within the polymer donor matrices strongly impedes the formation of proper bulk heterojunction (BHJ) morphology for efficient charge separation and transport, thereby limits the photovoltaic performance of the derived solar cells.[4]

To alleviate this problem, several approaches have been employed to modulate the intermolecular π–π stacking of PDI derivatives to achieve optimal BHJ morphology, such as introducing substituents at the imide, bay, or headland

C.-H. Wu, Dr. C.-C. Chueh, Dr. H.-L. Zhong, Prof. A. K.-Y. Jen
Department of Materials Science and Engineering
University of Washington
Seattle, WA 98195, USA
E-mail: ajen@u.washington.edu
C.-H. Wu, Prof. T.-C. Wen
Department of Chemical Engineering
National Cheng Kung University
Tainan 70101, Taiwan
Y.-Y. Xi, Prof. L. D. Pozzo
Department of Chemical Engineering
University of Washington
Seattle, WA 98195, USA

G.-P. Gao, Prof. Z.-H. Wang
State Key Laboratory of Organic Solids
Beijing National Laboratory for Molecular Sciences
Institute of Chemistry
Chinese Academy of Sciences
Beijing 100190, P. R. China
Prof. T.-C. Wen
Advanced Optoelectronic Technology Center
National Cheng Kung University
Tainan 70101, Taiwan

www.MaterialsViews.com

ADVANCED
FUNCTIONAL
MATERIALS
www.afm-journal.de

FULL PAPER

positions of PDI monomers,[5] creating PDI dimers (di-PDIs),[6,7] and 3D structure PDI-based acceptors.[8] Notably, two PDI monomers can be connected through various functional linkers at the bay positions to form bay-linked di-PDIs (B-di-PDIs). Since the functional linker will influence the twisting angle between the two PDI units, the B-di-PDIs show diverse absorption profile, charge transport, and molecular packing behavior.[6] With these endeavors, several B-di-PDIs-based PSCs have shown promising PCEs of ≈6%, which are among the highest values reported for the nonfullerene PSCs so far.[6g,9,10]

Compared to the B-di-PDIs, the hydrazine-linked analog (H-di-PDI), where the two PDI units are oriented perpendicularly to each other, are rarely explored to date. So far, it has only been successfully paired with one polymer donor to achieve a PCE of <5%.[7] The potential for H-di-PDI to achieve highly efficient nonfullerene PSCs might not be fully explored because it has only been screened with a few polymer donors. Therefore, it would be interesting to systematically compare H-di-PDI and B-di-PDI to understand the influence of molecular geometry on BHJ morphology and the device performance of derived PSCs.

In addition to developing nonfullerene acceptors, another important factor for achieving high-efficiency nonfullerene PSCs is the proper pairing with complementary polymer donors, especially with pseudo 2D conjugated polymers.[6g,9a,b,11] It has been reported that pseudo 2D conjugated polymers exhibit redshifted absorption and higher hole mobility than their 1D analogues.[12] More importantly, the conjugated side chains of these polymers can facilitate better compatibility with fullerene derivatives (such as $PC_{71}BM$) to achieve improved BHJ morphology.[13] Therefore, it will be interesting to learn if these side chains can also affect the interactions with di-PDI-based acceptors.

Two state-of-the-art polymer donors, PTB7 (1D) and PTB7-Th (2D), and their BHJ blends with H-di-PDI and B-di-PDI

acceptors were systematically investigated in this study (**Figure 1**).[6a,7,14] It was found that the PCE of the PTB7 derived PSC decreased significantly from 5.0% to 1.7% while the nonfullerene acceptor changed from B-di-PDI to H-di-PDI. However, the PCE of the PTB7-Th and H-di-PDI derived PSC increased significantly to 6.4% which is among the highest values reported so far for nonfullerene PSCs.[6g,9,10] These results suggest that 2D-conjugated side chains of the polymer donors improves the miscibility with di-PDI-based acceptors to minimize the dependence on their geometries. To prove this point, the influence of molecular geometry of the di-PDI-based acceptors on device performance was also investigated to correlate with the packing of polymer donors in BHJ films using 2D grazing incident wide-angle X-ray scattering (GIWAXS). The relatively flexible, twisted structure of B-di-PDI was found to disrupt the π–π stacking of PTB7-Th, leading to lower electron (μ_e) and hole mobilities (μ_h) in the derived BHJ device compared to those of PTB7-Th:H-di-PDI devices. The H-di-PDI acceptor could not only mix well with PTB7-Th but also maintained appropriate aggregation domains to facilitate efficient exciton dissociation and suitable percolation pathways for charge transport. This work reveals that both the conjugated side chains of polymer donors and the molecular geometry of di-PDI-based acceptors play important roles on affecting the derived BHJ morphology and device performance.

2. Results and Discussion

In this study, the relatively flexible B-di-PDI acceptor having a 70° torsion angle between the two constituent PDI units was used to compare with the rigid H-di-PDI acceptor which has a 90° torsion angle (Figure 1).[6] As shown in Figure S1
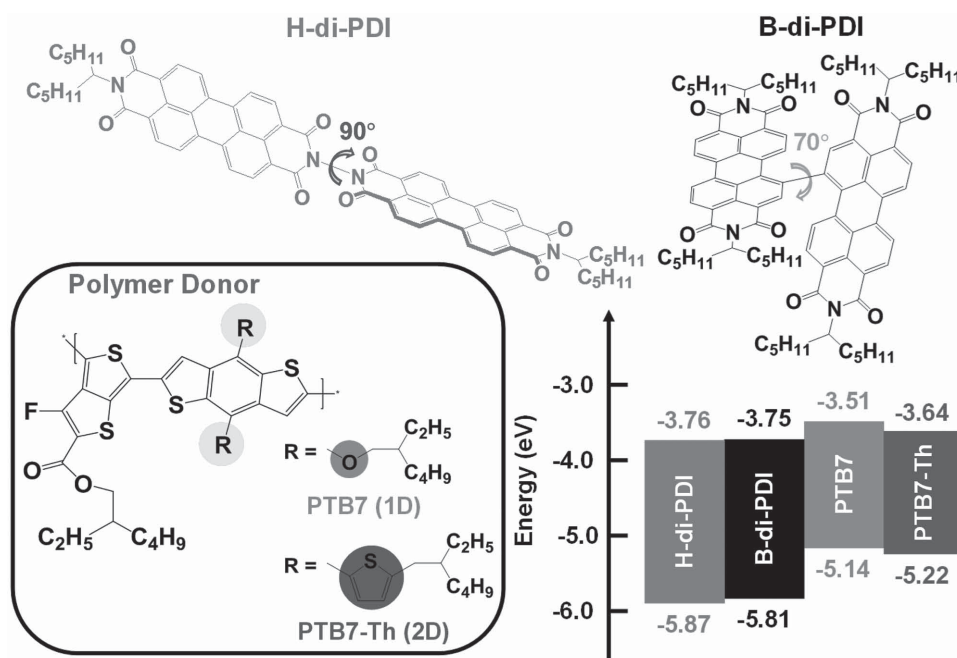

Figure 1. Molecular structures and the corresponding energy levels of the studied polymer donors and di-PDI-based acceptors.
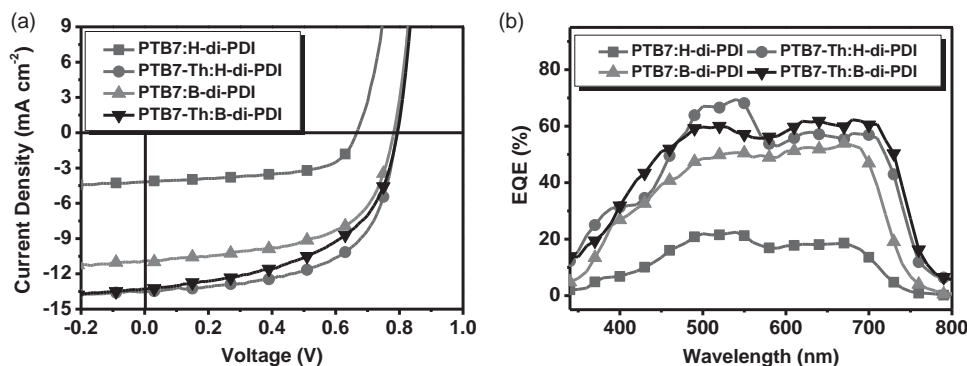
Figure 2. a) J–V characteristics and b) EQE spectra of the studied devices.

(Supporting Information), both di-PDI-based acceptors show intense narrow-band absorption ranging from 400 to 600 nm. Their complementary absorption to that of PTB7 and PTB7-Th is beneficial to form a BHJ layer having a broadband light harvesting. The cyclic voltammetry (CV) of both di-PDI-based acceptors are presented in Figure S2 (Supporting Information), which reveals nearly identical reduction potentials. The corresponding energy levels of all studied compounds are summarized in Figure 1. The similar energy levels between B-di-PDI and H-di-PDI allow us to directly correlate their differently molecular geometries with the optimized BHJ morphology and photovoltaic performance.

The solar cells in this study were fabricated in the inverted configuration of ITO/ZnO/nonfullerene BHJ/MoO$_3$/Ag, which is similar to that reported in our previous work.[9b] The optimized donor/acceptor (D/A) ratio for all nonfullerene BHJs is 1:1 with 1,8-diiodooctane (DIO) (1 vol%) and 1-chloronaphthalene (CN) (2 vol%) as solvent additives to promote optimal BHJ morphology.[9b] The thickness of all BHJ layers is controlled to be around 90 nm. The corresponding J–V curves of the studied devices are illustrated in **Figure 2**a and the detailed photovoltaic parameters are summarized in **Table 1**. As shown, the PTB7-based BHJ device exhibits dramatically different device performance when the acceptor was changed from B-di-PDI to H-di-PDI. The PTB7:B-di-PDI device showed a decent PCE$_{MAX}$ of 5.00% with a J_{SC} of 10.51 mA cm^{-2}, a V_{OC} of 0.78 V, and an FF of 0.58, but the PTB7:H-di-PDI device exhibited a much poor PCE$_{MAX}$ of 1.69% with a J_{SC} of 3.66 mA cm^{-2}, a V_{OC} of 0.79 V, and an FF of 0.51.

Providing that components in these blends have similar energy levels, the much lower J_{SC} found in the PTB7:H-di-PDI device indicates that it has significantly deteriorated BHJ morphology. Interestingly, the results from PTB7-Th with extended conjugated side chains are superior to those from PTB7 which is consistent with what we observed from our previous work.[9b] The PTB7-Th:B-di-PDI device afforded a high PCE$_{MAX}$ of 5.56% with a J_{SC} of 12.86 mA cm^{-2}, a V_{OC} of 0.79 V, and an FF of 0.54 while the PTB7-Th:H-di-PDI device delivered an even higher PCE$_{MAX}$ of 6.41% with a J_{SC} of 13.12 mA cm^{-2}, a V_{OC} of 0.79 V, and an FF of 0.60. The higher PCEs obtained in PTB7-Th-based devices signify that there is less geometric dependency for di-PDI-based acceptors on pseudo 2D donor system in forming optimal BHJ morphology. In addition to the advantages of forming better BHJ morphology, the redshifted absorption of PTB7-Th might also contribute to the superior PCEs.

Apart from the structure differences in polymer donors, the molecular geometry of the di-PDI acceptors may also play an important role in affecting the resultant device performance. The B-di-PDI acceptor can be blended with both polymer donors to afford respectful PCEs (5.00% with PTB7:B-di-PDI and 5.56% with PTB7-Th:B-di-PDI), suggesting the relatively flexible and twisted B-di-PDI have better miscibility with different geometries polymer donors. On the contrary, the H-di-PDI acceptor can only afford high PCE with the PTB7-Th system due to its high rigidity. Once the geometric dependence of the polymer donor (1D PTB7 herein) increases, the miscibility between them becomes a severe issue, which results in decreased PCE. It is important to point out that high PCE observed in the PTB7-Th:H-di-PDI device is among the highest reported so far in the nonfullerene PSCs.[6g,9,10] This suggests that the highly rigid H-di-PDI can still mix well with the PTB7-Th to afford appropriate sized aggregation domains to enable efficient exciton dissociation and suitable charge transport.

Figure 2b shows the external quantum efficiency (EQE) spectra of the studied devices. The broadband spectra show both polymer donors and nonfullerene acceptors contribute to the generation of excitons in devices. Impressively, the highest EQE value of the top-performing PTB7-Th:H-di-PDI device reaches 70% at 540 nm. Besides, both PTB7-Th-based devices show higher EQE values than those of PTB7-based ones across the 470–800 nm region, confirming more efficient exciton dissociation and charge transport in the BHJs.
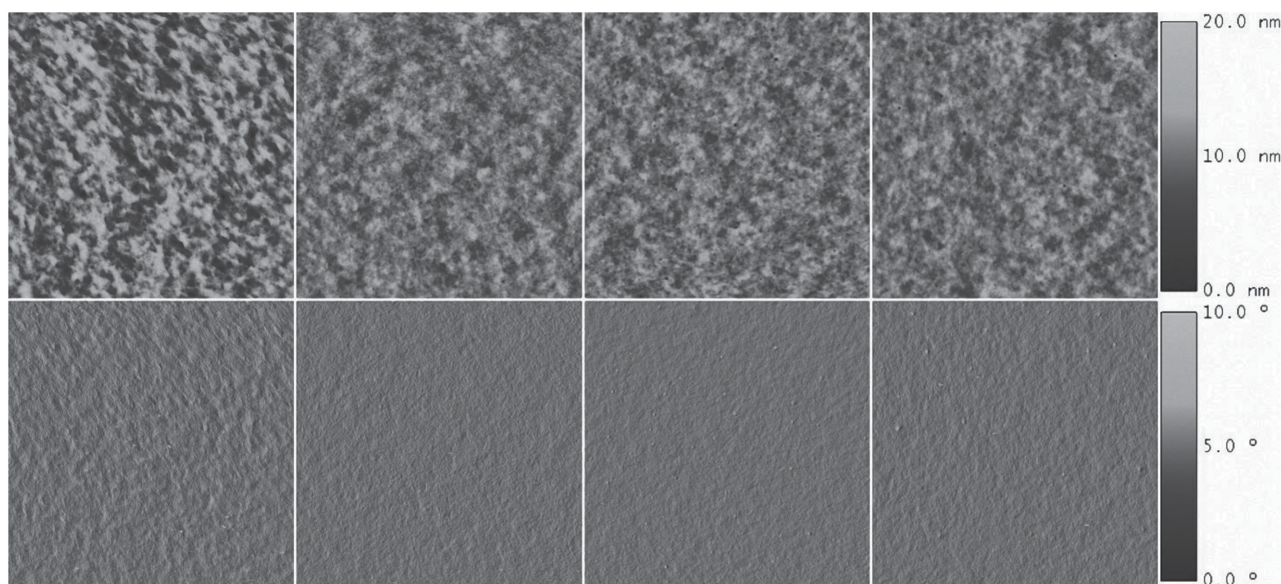
Table 1. Photovoltaic performance for the studied devices. The average values are collected from six independent devices.

Acceptor	V_{OC} [V]	J_{SC} [mA cm^{-2}]	FF	PCE [%]	PCE$_{MAX}$ [%]
Donor: PTB7					
B-di-PDI	0.78 ± 0.00	10.51 ± 0.22	0.58 ± 0.01	4.77	5.00
H-di-PDI	0.79 ± 0.00	3.66 ± 0.14	0.51 ± 0.02	1.47	1.69
Donor: PTB7-Th					
B-di-PDI	0.79 ± 0.00	12.86 ± 0.29	0.54 ± 0.01	5.45	5.56
H-di-PDI	0.79 ± 0.00	13.12 ± 0.33	0.60 ± 0.01	6.19	6.41

Materials
Views
www.MaterialsViews.com

ADVANCED
FUNCTIONAL
MATERIALS
www.afm-journal.de

FULL PAPER

Figure 3. The AFM a–d) height and e–h) phase images of a,e) PTB7:H-di-PDI, b,f) PTB7-Th:H-di-PDI, c,g) PTB7:B-di-PDI, and d,h) PTB7-Th:B-di-PDI blend films.

Atomic force microscopy (AFM) was conducted to probe the surface morphology of the studied BHJ layers (**Figure 3**). It was revealed that the PTB7:H-di-PDI film possesses the roughest surface with a root mean square roughness (R_{rms}) of 3.22 nm while the other films show relatively smoother surface, where the R_{rms} for PTB7-Th:H-di-PDI, PTB7:B-di-PDI, and PTB7-Th:B-di-PDI films are 1.78, 1.82, and 1.71 nm, respectively. The relatively large phase separation observed in the PTB7:H-di-PDI film indicates that inferior intermixing between H-di-PDI and 1D PTB7 than the other BHJ films, probably due to higher intrinsic aggregation tendency of H-di-PDI (Figure S3, Supporting Information).

Steady-state photoluminescence (PL) spectroscopy was also employed to investigate charge dissociation in the BHJ films to provide better understanding of the degree of intermixing between polymer donors and di-PDI-based acceptors.[7b,10c] The PL spectra of the di-PDI-based acceptors and polymer donors are shown in **Figure 4** and Figure S4 (Supporting Information), respectively, and the detailed PL quenching efficiencies are summarized in **Table 2**. Due to the inferior BHJ morphology revealed previously, the PTB7:H-di-PDI film shows the lowest PL quenching efficiency among the studied BHJ films, confirming the poorer miscibility between PTB7 and H-di-PDI. This morphology also results in lower J_{SC} due to less donor/acceptor (D/A) interfaces in the BHJ film.

Noticeably, all the PTB7-Th-based BHJ films have higher PL quenching efficiency than the PTB7-based BHJ films. This might be due to the conjugated side chains of PTH7-Th provide more effective interactions with the di-PDI-based acceptors to afford sufficient D/A interfaces for efficient exciton dissociation to reduce the geometrical dependence of the nonfullerene acceptors. On the other hand, both B-di-PDI derived films show efficient PL quenching, suggesting that the relatively flexible B-di-PDI can mix well with polymer donors despite of their dimensionality. However, the PTB7-Th:H-di-PDI film even shows enhanced hole transfer quenching compared to that of PTB7-Th:B-di-PDI film while maintaining comparable electron transfer quenching. These validate the
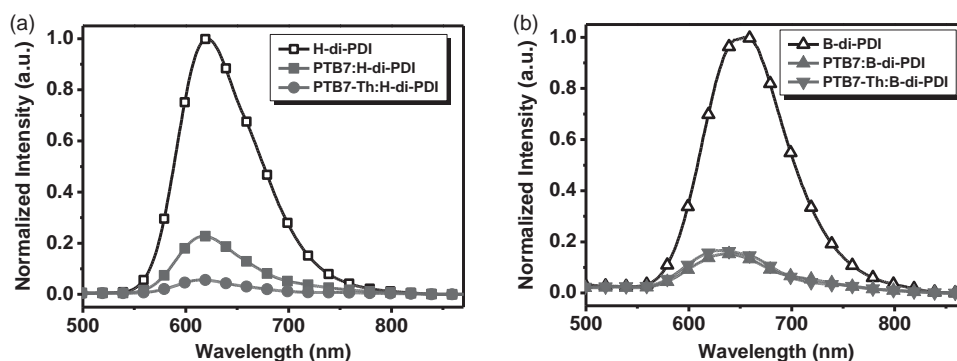

Figure 4. Steady-state PL quenching spectra of a) H-di-PDI and its derived BHJs blended with PTB7 and PTB7-Th and b) B-di-PDI and its derived BHJs blended with PTB7 and PTB7-Th. The excitation wavelength is 457 nm.

Table 2. PL quenching efficiency of the studied blend films.

	PL quenching efficiency [%]	
	Hole transfer (excitons from acceptors)	Electron transfer (excitons from donors)
PTB7:H-di-PDI	77	83
PTB7-Th:H-di-PDI	95	92
PTB7:B-di-PDI	85	96
PTB7-Th:B-di-PDI	87	97

Table 3. Hole and electron mobilities of all derived devices.

	μ_h [cm^2 V^{-1} s^{-1}]	μ_e [cm^2 V^{-1} s^{-1}]	μ_h/μ_e ratio
PTB7:H-di-PDI	3.5×10^{-3}	–	–
PTB7-Th:H-di-PDI	2.3×10^{-2}	4.3×10^{-4}	53
PTB7:B-di-PDI	6.3×10^{-3}	8.1×10^{-5}	78
PTB7-Th:B-di-PDI	1.7×10^{-2}	9.4×10^{-5}	181

hypothesis that the relatively rigid H-di-PDI not only can mix well with PTB7-Th but also can form appropriate aggregation domains to enable efficient exciton dissociation and charge transport.

To probe the charge-transporting behavior of studied BHJ layers, the hole (μ_h) and electron (μ_e) mobilities were further evaluated by measuring the space-charge-limited current (SCLC) and the results are presented in **Figure 5** and **Table 3**. As shown, all the BHJ films exhibited higher μ_h than μ_e, indicating that μ_e is the limiting factor for achieving high J_{SC} and FF. It is important to note that the electron-only device derived from PTB7:H-di-PDI shows much lower current density than the others (not shown here) due to its inferior BHJ morphology. All the PTB7-Th-based devices showed higher charge mobility than those of the PTB7-based devices, affirming that conjugated side chains of PTB7-Th facilitate the formation of optimized percolation pathways for charge transport.[15]

To gain more insight of polymer/acceptor π–π stacking in the PTB7-Th:H-di-PDI and PTB7-Th:B-di-PDI devices, 2D GIWAXS was employed and the results of the neat PTB7-Th film, PTB7-Th:H-di-PDI film, and PTB7-Th:B-d-iPDI film are shown in **Figure 6**. The PTB7-Th:H-di-PDI film shows a comparable peak intensity of the face-on oriented π–π stacking to that of the neat PTB7-Th film, whereas the PTB7-Th:B-di-PDI film exhibits a lower peak intensity of the face-on oriented π–π stacking. It is known that such face-on oriented π–π stacking is favorable to efficient charge transport and collection.[16] This result verified that the face-on oriented π–π stacking of PTB7-Th was not severely disrupted after blending with H-di-PDI, probably due to its high rigidity relative to B-di-PDI.

3. Conclusion

We have systematically investigated the influence of molecular geometry of the polymer donors and the di-PDI-based acceptors on BHJ morphology of the nonfullerene PSCs. The results reveal that polymer donors with 2D conjugated side chains significantly enhance the miscibility with di-PDI-based acceptors. The effect of molecular geometry of di-PDI-based acceptors on device performance was investigated by GIWAXS and showed that it is greatly influenced by packing of polymer donors in the BHJ film. The relatively flexible, twisted B-di-PDI was found to disrupt the π–π stacking of PTB7-Th, while the rigid H-di-PDI was found to not only have good miscibility with PTB7-Th but also maintain appropriate aggregation domains to enable efficient exciton dissociation and suitable percolation pathways for charge transport. As a result, a very promising PCE of 6.41% was achieved in the PTB7-Th:H-di-PDI BHJ device, which is among the highest values reported so far for the nonfullerene PSCs.

4. Experimental Section

Materials and Characterization: PC$_{71}$BM and PTB7/PTB7-Th are purchased from American Dye Source and 1-Material, Inc, respectively. Both B-di-PDI and H-di-PDI are synthesized using methods reported in the literature. Unless otherwise specified, chemicals, and solvents were purchased from Aldrich. UV–vis spectra and PL spectra were recorded with Varian Cary 5000 UV–vis–NIR and Horiba Fluorolog FL-3, respectively. AFM images were obtained by using a NanoScope IIIa (Digital instrument Inc.) operated in the tapping mode. GIWAXS
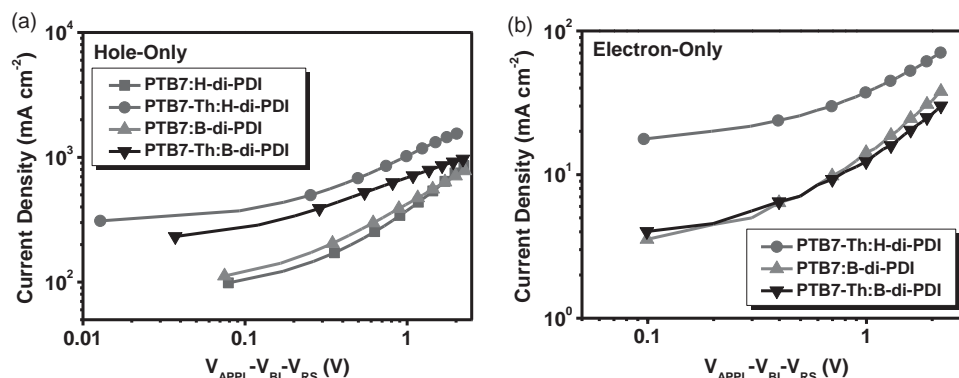

Figure 5. Measured space-charge-limited *J*–*V* characteristics of all the derived blends under dark conditions for a) hole-only devices and b) electron-only devices.

www.MaterialsViews.com

ADVANCED
FUNCTIONAL
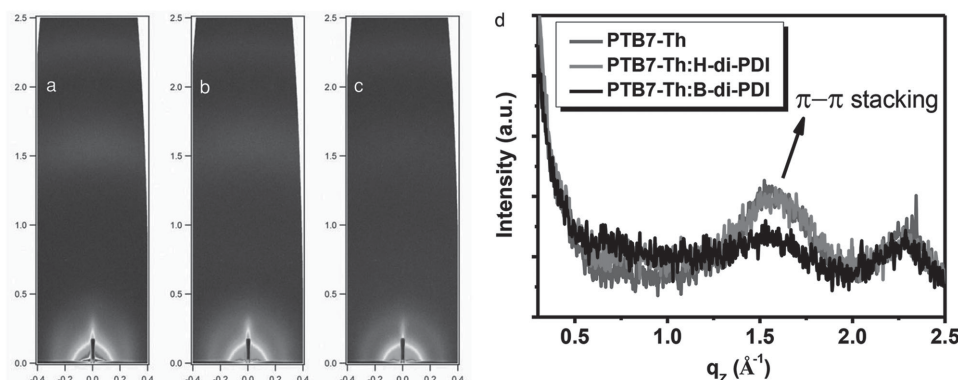MATERIALS
www.afm-journal.de

FULL PAPER

Figure 6. 2D GIWAXS images of a) the neat PTB7-Th film, b) PTB7-Th:H-di-PDI film, and c) PTB7-Th:B-di-PDI film. d) The corresponding intensity along the q_z direction (out plane).

measurements were conducted with Anton Paar SAXSess instrument. The wavelength of the X-ray (Cu Kα) was 1.54 Å. The neat polymer or nonfullerene BHJ ($\approx$90–100 nm) were spin coated on the Si/ZnO chips with 1.5 cm $\times$ 1.5 cm size. They were aligned and tilted with a 0.19° angle by using pin diode. The 2D scattering patterns were recorded on wide-angle image plates for 15 h. The reduction of the GIWAXS data was within the framework of Distorted Wave Born Approximation (DWBA), which enables the analytical treatment of the scattering intensity. Custom IGOR Pro reduction macros were utilized to convert pixel positions on each raw scattering image to intensity versus Qy and Qz with respect to the sample reference plane. All the scattering intensity was normalized to scattering time. The 1D scattering curve was obtained by integration along Qy = 0 on the 2D Qy, Qz plot.[17]

Device Fabrication: ITO-coated glass substrates (15 Ω sq^{-1}) were cleaned ultrasonically with detergent, deionized water, acetone, and isopropyl alcohol in sequence for 10 min each. Subsequently, they were treated with oxygen plasma for 1 min. A ZnO precursor solution was spin coated onto precleaned ITO-coated glass substrates at 4000 rpm for 60 s and then annealed at 200 °C for 1 h in air to complete the thin layer of ZnO ($\approx$30 nm). The ZnO precursor solution was prepared by dissolving zinc acetate dehydrate $C_4H_6O_4Zn \cdot 2(H_2O)$ (99.5%, Merck 1 g) and ethanolamine ($HOCH_2CH_2NH_2$, 98% Acros, 0.28 g) in 2-methoxyethanol ($CH_3OCH_2CH_2OH$, Aldrich, 98%, 10 mL) under stirring for 8 h for hydrolysis reaction and aging. The active layers ($\approx$90 nm) were obtained by spin-coating the active layer solution that was filtered with a PTFE (polytetrafluoroethylene) filter (0.45 μm) atop the thin layer of ZnO. The donor:acceptor blends with 1:1 ratio were dissolved in DCB with 1% DIO and 2% CN and stirred overnight in a nitrogen-filled glove box. The anode of each device, MoO$_3$/Ag (8 nm/150 nm), was thermally evaporated at a pressure of about 10^{-7} Torr. The area of each device was 3.14 mm^2 defined by a shadow mask. Electron-only devices with the configuration of ITO/ZnO/nonfullerene BHJ/Ca (20 nm)/Al (130 nm) and hole-only devices with the configuration of ITO/PEDOT:PSS/nonfullerene BHJ/MoO$_3$/Ag were used to evaluate charge mobilities by SCLC model.

Device Characterization: The J–V characteristics of devices under an AM 1.5 G illumination of 100 mW cm^{-2} were measured by using a Keithley 2400 source-measure unit in a nitrogen-filled glove box. Devices were measured without any shadow masking. The AM 1.5 G illumination was simulated by using an Oriel 300 W Solar Simulator and calibrated by using a silicon photodiode with a protective KG5 filter calibrated by the National Renewable Energy Laboratory (NREL). The EQE system uses a lock-in amplifier (Stanford Research Systems SR830) to record the short-circuit current under chopped monochromatic light. The charge mobilities were determined by fitting the dark current according to the following equation

$$J(V) = \frac{9V^2}{8L^3} \varepsilon_0 \varepsilon_r \mu_0 \, e^{\left(0.89\gamma\sqrt{V/L}\right)} \tag{1}$$

where J is the dark current density (mA cm^{-2}), μ_0 is the zero-field mobility (cm^2 V^{-1} s^{-1}), ε_0 is the permittivity of free space (88.54 $\times$ 10^{-12} mA s V^{-1} s^{-1}), ε_r is the relative permittivity of the material (3), V is the effective voltage ($V = V_{Applied} - V_{Built-in} - V_{series\ resistane}$), and L is the thickness of the active layer.

Supporting Information

Supporting Information is available from the Wiley Online Library or from the author.

Acknowledgements

[1] a) Y. H. Liu, J. B. Zhao, Z. K. Li, C. Mu, W. Ma, H. W. Hu, K. Jiang, H. R. Lin, H. Ade, H. Yan, *Nat. Commun.* **2014**, *5*, 5293; b) Z. C. He, B. Xiao, F. Liu, H. B. Wu, Y. L. Yang, S. Xiao, C. Wang, T. P. Russell, Y. Cao, *Nat. Photonics* **2014**, *9*, 174.

[2] a) A. F. Eftaiha, J. P. Sun, I. G. Hill, G. C. Welch, *J. Mater. Chem. A* **2014**, *2*, 1201; b) Y. Z. Lin, X. W. Zhan, *Mater. Horiz.* **2014**, *1*, 470.

[3] a) C. H. Woo, T. W. Holcombe, D. A. Unruh, A. Sellinger, J. M. J. Frechet, *Chem. Mater.* **2010**, *22*, 1673; b) Y. Zhou, Y. Z. Dai, Y. Q. Zheng, X. Y. Wang, J. Y. Wang, J. Pei, *Chem. Commun.* **2013**, *49*, 5802; c) Y. Z. Lin, P. Cheng, Y. F. Li, X. W. Zhan, *Chem. Commun.* **2012**, *48*, 4773; d) E. Ahmed, G. Q. Ren, F. S. Kim, E. C. Hollenbeck, S. A. Jenekhe, *Chem. Mater.* **2011**, *23*, 4563; e) E. Kozma, M. Catellani, *Dyes Pigm.* **2013**, *98*, 160.

[4] a) J. J. Dittmer, E. A. Marseglia, R. H. Friend, *Adv. Mater.* **2000**, *12*, 1270; b) J. E. Anthony, *Chem. Mater.* **2011**, *23*, 583.

[5] a) C. Li, H. Wonneberger, *Adv. Mater.* **2012**, *24*, 613; b) V. Kamm, G. Battagliarin, I. A. Howard, W. Pisula, A. Mavrinskiy, C. Li, K. Mullen, F. Laquai, *Adv. Energy Mater.* **2011**, *1*, 297;

c) P. E. Hartnett, A. Timalsina, H. S. S. R. Matte, N. J. Zhou, X. G. Guo, W. Zhao, A. Facchetti, R. P. H. Chang, M. C. Hersam, M. R. Wasielewski, T. J. Marks, *J. Am. Chem. Soc.* **2014**, *136*, 16345.

[6] a) W. Jiang, L. Ye, X. G. Li, C. Y. Xiao, F. Tan, W. C. Zhao, J. H. Hou, Z. H. Wang, *Chem. Commun.* **2014**, *50*, 1024; b) B. Jiang, X. Zhang, C. L. Zhan, Z. H. Lu, J. H. Huang, X. L. Ding, S. G. He, J. N. Yao, *Polym. Chem.* **2013**, *4*, 4631; c) Z. H. Lu, X. Zhang, C. L. Zhan, B. Jiang, X. L. Zhang, L. L. Chen, J. N. Yao, *Phys. Chem. Chem. Phys.* **2013**, *15*, 11375; d) X. Zhang, Z. H. Lu, L. Ye, C. L. Zhan, J. H. Hou, S. Q. Zhang, B. Jiang, Y. Zhao, J. H. Huang, S. L. Zhang, Y. Liu, Q. Shi, Y. Q. Liu, J. N. Yao, *Adv. Mater.* **2013**, *25*, 5791; e) Q. F. Yan, Y. Zhou, Y. Q. Zheng, J. Pei, D. H. Zhao, *Chem. Sci.* **2013**, *4*, 4389; f) Y. Z. Lin, J. Y. Wang, S. X. Dai, Y. F. Li, D. B. Zhu, X. W. Zhan, *Adv. Energy Mater.* **2014**, *4*, 1400420; g) Y. Zhong, M. T. Trinh, R. S. Chen, W. Wang, P. P. Khlyabich, B. Kumar, Q. Z. Xu, C. Y. Nam, M. Y. Sfeir, C. Black, M. L. Steigerwald, Y. L. Loo, S. X. Xiao, F. Ng, X. Y. Zhu, C. Nuckolls, *J. Am. Chem. Soc.* **2014**, *136*, 15215.

[7] a) S. Rajaram, R. Shivanna, S. K. Kandappa, K. S. Narayan, *J. Phys. Chem. Lett.* **2012**, *3*, 2405; b) R. Shivanna, S. Shoaee, S. Dimitrov, S. K. Kandappa, S. Rajaram, J. R. Durrant, K. S. Narayan, *Energy Environ. Sci.* **2014**, *7*, 435; c) R. Shivanna, S. Rajaram, K. S. Narayan, *Appl. Phys. Lett.* **2015**, *106*, 123301.

[8] a) Y. Z. Lin, Y. F. Wang, J. Y. Wang, J. H. Hou, Y. F. Li, D. B. Zhu, X. W. Zhan, *Adv. Mater.* **2014**, *26*, 5137; b) Y. H. Liu, C. Mu, K. Jiang, J. B. Zhao, Y. K. Li, L. Zhang, Z. K. Li, J. Y. L. Lai, H. W. Hu, T. X. Ma, R. R. Hu, D. M. Yu, X. H. Huang, B. Z. Tang, H. Yan, *Adv. Mater.* **2015**, *27*, 1015; c) S. Y. Liu, C. H. Wu, C. Z. Li, S. Q. Liu, K. H. Wei, H. Z. Chen, A. K. Y. Jen, *Adv. Sci.* **2015**, *2*, 1500014.

[9] a) X. Zhang, C. L. Zhan, J. N. Yao, *Chem. Mater.* **2015**, *27*, 166; b) Y. Zang, C. Z. Li, C. C. Chueh, S. T. Williams, W. Jiang, Z. H. Wang, J. S. Yu, A. K. Y. Jen, *Adv. Mater.* **2014**, *26*, 5708; c) J. B. Zhao, Y. K. Li, H. R. Lin, Y. H. Liu, K. Jiang, C. Mu, T. X. Ma, J. Y. L. Lai, H. Yan, *Energy Environ. Sci.* **2015**, *8*, 520.

[10] a) Y. Z. Lin, Z. G. Zhang, H. T. Bai, J. Y. Wang, Y. H. Yao, Y. F. Li, D. B. Zhu, X. W. Zhan, *Energy Environ. Sci.* **2015**, *8*, 610; b) Y. Z. Lin, J. Y. Wang, Z. G. Zhang, H. T. Bai, Y. F. Li, D. B. Zhu, X. W. Zhan, *Adv. Mater.* **2015**, *27*, 1170; c) C. Lee, H. Kang, W. Lee, T. Kim, K. H. Kim, H. Y. Woo, C. Wang, B. J. Kim, *Adv. Mater.* **2015**, *27*, 2466.

[11] a) L. Ye, W. Jiang, W. C. Zhao, S. Q. Zhang, D. P. Qian, Z. H. Wang, J. H. Hou, *Small* **2014**, *10*, 4658; b) L. Ye, W. Jiang, W. C. Zhao, S. Q. Zhang, Y. Cui, Z. H. Wang, J. H. Hou, *Org. Electron.* **2015**, *17*, 295.

[12] L. Ye, S. Q. Zhang, L. J. Huo, M. J. Zhang, J. H. Hou, *Acc. Chem. Res.* **2014**, *47*, 1595.

[13] S. Q. Zhang, L. Ye, Q. Wang, Z. J. Li, X. Guo, L. J. Huo, H. L. Fan, J. H. Hou, *J. Phys. Chem. C* **2013**, *117*, 9550.

[14] S. H. Liao, H. J. Jhuo, Y. S. Cheng, S. A. Chen, *Adv. Mater.* **2013**, *25*, 4766.

[15] a) I. A. Howard, F. Laquai, P. E. Keivanidis, R. H. Friend, N. C. Greenham, *J. Phys. Chem. C* **2009**, *113*, 21225; b) M. G. Li, J. G. Liu, X. X. Cao, K. Zhou, Q. Q. Zhao, X. H. Yu, R. B. Xing, Y. C. Han, *Phys. Chem. Chem. Phys.* **2014**, *16*, 26917.

[16] C. Piliego, T. W. Holcombe, J. D. Douglas, C. H. Woo, P. M. Beaujuge, J. M. J. Frechet, *J. Am. Chem. Soc.* **2010**, *132*, 7595.

[17] J. J. Richards, *Ph.D. Thesis*, University of Washington (Seatlle, WA, USA) **2014**.